Pergamon

Int. J. Solids Structures Vol. 34, Nos. 35–36, pp. 4463–4478, 1997

0020–7683/97 $17.00 + .00

PII: S0020–7683(97)00053–X

ELASTIC FIELD OF A THIN-FILM/SUBSTRATE SYSTEM UNDER AN AXISYMMETRIC LOADING

JACKIE LI and TSU-WEI CHOU
Center for Composite Materials and Department of Mechanical Engineering, University of Delaware, Newark, DE 19716, U.S.A.

(*Received* 22 *July* 1996, *in revised form* 29 *January* 1997)

Abstract—This paper presents the elastic solution of a layered half space with perfect interfacial bonding under an axisymmetrical compressive loading on the plane surface. The analysis is intended to model the nano-indentation of thin-film coating/substrate systems. Unlike most of the existing work of which the substrate is assumed as rigid and the numerical results are obtained by finite element analysis, the present paper presents theoretical solutions for the elastic coating/substrate systems. The surface displacement profiles and the stress fields are shown to be sensitive to the thickness of the coating layer and the ratio of the elastic modulus of the coating material to that of the substrate. When the film thickness is comparable to the loading contact radius, the film elastic property cannot be accurately determined by using Sneddon's half-space indentation solution. Furthermore, there are pronounced differences in the stress fields of the hard-coating and the soft-coating systems. When an indentation load is applied to a soft-thin-film/hard-substrate system, most the stress components are compressive. But for a hard-thin-film/soft-substrate system, the radial and hoop stresses in the film near the film/substrate interface change from tension to compression as the film thickness decreases. The normal and shear stress results are compared with those obtained from finite element analysis (Jayachandran, R., Boyce, M. C. and Argon, A. S. (1995) Mechanics of the indentation test and its use to assess the adhesion of polymeric coatings. In *Adhesion Measurement of Films and Coatings*, ed. K. L. Mittal. VSP, pp. 189–215) for the rigid substrate system. Also, the load-indentation depth results are compared with the experimental data of Oliver and Pharr (Oliver, W. C. and Pharr, G. M. (1992) An improved technique for determining hardness and elastic modulus using load and displacement sensing indentation experiments. *Journal of Material Research* 7(6), 1564–1583) for tungsten subjected to elastic indentation. The agreement is quite satisfactory. Implications of the elastic field on the failure mechanisms of coating/substrate systems are also discussed. © 1997 Elsevier Science Ltd.

1. INTRODUCTION

Indentation tests have been widely used to measure the elastic and fracture behaviour of solids and examine the adhesion between coatings and substrates. Sneddon and co-workers (1945, 1948, 1951 and 1965) have systematically studied the indentation problems of a homogeneous material by using Hankel's transforms. Their elegant results can be used to determine the hardness and elastic Young's modulus of the material (see, for example, Doerner and Nix, 1986 and Oliver and Pharr, 1992). The indentation problems have also been studied using contact mechanics approach. A comprehensive study of contact mechanics can be found in the book by Johnson (1985).

When a solid thin film is deposited over a substrate, the problem becomes much more complex. The elastic response of coating/substrate systems subjected to indentation can be categorized according to the coating material: in one case the coating material is not as stiff as the substrate and in the other case the thin film is stiffer. For the first type of coating/substrate system, the substrate has usually been approximated as rigid by most researchers. For instance, Matthewson (1981) analyzed the indentation of a soft coating/rigid substrate system. Ritter *et al.* (1989) and Lin *et al.* (1990) used indentation techniques to measure the adhesion and interfacial shear strength of thin polymer coatings on glass and then compared the experimental results to Matthewson's (1981) analytical predictions. Numerical simulations of soft-coating/rigid-substrate systems using the finite element method have also been carried out by Jayachandran *et al.* (1995), among others.

However, the substrate is not ideally rigid in reality, and its elastic properties cannot be disregarded when a soft coating is applied to it. With the increased use of hard-coatings on soft-substrates such as diamond-like coatings on metal substrates in cutting tools and corrosion- and erosion-resistant coatings, a proper evaluation of their mechanical behavior requires knowledge of the effects of elastic properties of both the coating and the substrate. In addition, the thickness of the coating and the contact loading radius are critical parameters that must be fully accounted for. Such problems have received considerable attention in the literature. Chui and Hartnett (1983) used the numerical iterations based on the generalized Boussinesq solution for a point force to evaluate the elastic contact problems of the layered materials. Van der Zwaag and Field (1982, 1983) investigated the effect of thin hard-coatings on Hertzian stress field under spherical indentation using finite element analysis and experimental liquid impact testing. O'Sullivan and King (1988) studied the sliding contact stress field due to a spherical indenter on the layered elastic half-space using a least-squares iterative approach by the Papkovich–Neuber potentials. Komvopoulos and co-workers (1987, 1988, 1989, 1995) have performed finite element analysis on the layered substrate materials under cylindrical and spherical indentations. Van der Zwaag *et al.* (1986) and Lardner *et al.* (1992) also studied the contact stress in double layered hard coating by finite element analysis.

In this study, we solve the elastic problem of thin-film coating/substrate systems analytically by using the Hankel's transform method. The evaluation of the displacement, stress field, and load-indentation depth relation of the thin-film/substrate system under an axisymmetrically distributed loading on the plane surface of the film has been carried out.

2. ANALYSIS

In the thin-film/substrate system shown in Fig. 1, the thin-film coating is referred to as phase 1 and the substrate as phase 0. For simplicity, both phases are assumed to be isotropic, with Young's modulus and Poisson's ratio denoted by E_r and v_r, respectively, for the r-th phase; the shear modulus then follows as $\mu_r = E_r/(2(1+v_r))$. The thickness of the film is denoted as t. An arbitrary normal distributed stress with the loading contact radius

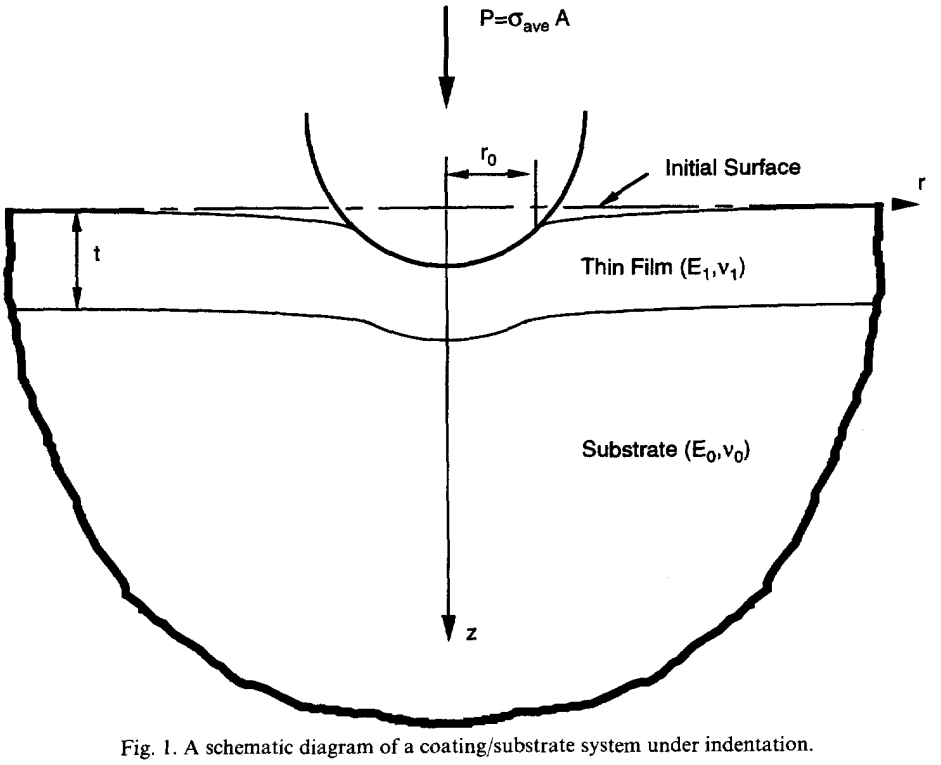

Fig. 1. A schematic diagram of a coating/substrate system under indentation.

r_0 is applied on the free surface symmetrically with respect to the z-axis. Here we use the cylindrical polar coordinates (r, θ, z) and denote the displacements as u, v and w along the r-, θ-, and z-directions, respectively. The stress components are denoted as σ_r, σ_θ, σ_z, $\tau_{r\theta}$, $\tau_{\theta z}$ and τ_{zr}.

The symmetry condition with respect to the z-axis implies that v, $\tau_{r\theta}$ and $\tau_{\theta z}$ all vanish and the equilibrium equations reduce to

$$\frac{\partial \sigma_r}{\partial r} + \frac{\partial \tau_{rz}}{\partial z} + \frac{1}{r}(\sigma_r - \sigma_\theta) = 0 \tag{1}$$

$$\frac{\partial \tau_{rz}}{\partial r} + \frac{\partial \sigma_z}{\partial z} + \frac{\tau_{zr}}{r} = 0. \tag{2}$$

The equilibrium equations and compatibility equations in cylindrical coordinates are satisfied by a stress function, which is a solution of the biharmonic equation. Then, by applying the method Hankel transforms, the biharmonic equation can be further reduced to an ordinary differential equation. The detail of the procedure can be found in Harding and Sneddon (1945). The expressions of displacements and stress components are recapitulated as follows:

$$u_i = \int_0^\infty \{[\xi^2 A_i + \xi(1+\xi z)B_i]\, e^{\xi z} + [-\xi^2 C_i + \xi(1-\xi z)D_i]\, e^{-\xi z}\}\xi J_1(\xi r)\, \mathrm{d}\xi \tag{3}$$

$$w_i = \int_0^\infty \{[-\xi^2 A_i + \xi(2-4\gamma_i-\xi z)B_i]\, e^{\xi z} + [-\xi^2 C_i - \xi(2-4\gamma_i+\xi z)D_i]\, e^{-\xi z}\}\xi J_0(\xi r)\, \mathrm{d}\xi \tag{4}$$

and

$$\sigma_{ri} = 2\mu_i \int_0^\infty \{[\xi^2 A_i + \xi(1+2\gamma_i+\xi z)B_i]\, e^{\xi z} + [-\xi^2 C_i + \xi(1+2\gamma_i-\xi z)D_i]\, e^{-\xi z}\}\xi^2 J_0(\xi r)\, \mathrm{d}\xi$$
$$- \frac{2\mu_i}{r} \int_0^\infty \{[\xi A_i + (1+\xi z)B_i]\, e^{\xi z} + [-\xi C_i + (1-\xi z)D_i]\, e^{-\xi z}\}\xi^2 J_1(\xi r)\, \mathrm{d}\xi \tag{5}$$

$$\sigma_{\theta i} = 2\mu_i\gamma_i \int_0^\infty 2(B_i e^{\xi z} + D_i e^{-\xi z})\xi^3 J_0(\xi r)\, \mathrm{d}\xi$$
$$+ \frac{2\mu_i}{r} \int_0^\infty \{[\xi A_i + (1+\xi z)B_i]\, e^{\xi z} + [-\xi C_i + (1-\xi z)D_i]\, e^{-\xi z}\}\xi^2 J_1(\xi r)\, \mathrm{d}\xi \tag{6}$$

$$\sigma_{zi} = 2\mu_i \int_0^\infty \{[-\xi^2 A_i + \xi(1-2\gamma_i-\xi z)B_i]\, e^{\xi z} + [\xi^2 C_i + \xi(1-2\gamma_i+\xi z)D_i]\, e^{-\xi z}\}\xi^2 J_0(\xi r)\, \mathrm{d}\xi \tag{7}$$

$$\tau_{zri} = 2\mu_i \int_0^\infty \{[\xi^2 A_i + \xi(2\gamma_i+\xi z)B_i]\, e^{\xi z} + [\xi^2 C_i - \xi(2\gamma_i-\xi z)D_i]\, e^{-\xi z}\}\xi^2 J_1(\xi r)\, \mathrm{d}\xi \tag{8}$$

where the subscript $i = 0, 1$ denoting the substrate and the film, respectively, J_m $(m = 0, 1)$ is a Bessel function of the first kind of order m, and the coefficients A_i, B_i, C_i and D_i $(i = 0, 1)$ can be determined from the boundary and interfacial continuity conditions. Since the components of stress and displacement approach zero as $z \to \infty$, A_0 and B_0 must be zero, and the eight coefficients reduce to six.

The original indentation problem for a homogeneous body discussed by Sneddon (1951) was a mixed boundary value problem. It was assumed that the z-component of the surface displacement w is specified by the shape of the indenter over the contact region $r < r_0$ of the surface ($z = 0$), while the region outside of the contact zone is stress-free. Due to the complexity of the indentation problem involved in a thin-film/substrate, an axisymmetrically distributed normal stress is considered in the present study instead:

$$\sigma_z(r,0) = -q(r), \quad \tau_{zr}(r,0) = 0 \tag{9}$$

on the free surface ($z = 0$). In eqn (9) the negative sign represents a compression, and the function $q(r)$ may be represented in an integral form which is also known as Hankel's transform

$$q(r) = \int_0^\infty \bar{q}(\xi)\xi J_0(\xi r)\,\mathrm{d}\xi. \tag{10}$$

We assume that the interface between the film and the substrate is perfectly bonded. Then the interfacial continuity conditions at the plane $z = t$ are given as

$$\begin{aligned} u_1(r,t) &= u_0(r,t) \qquad w_1(r,t) = w_0(r,t) \\ \sigma_{z1}(r,t) &= \sigma_{z0}(r,t) \quad \tau_{zr1}(r,t) = \tau_{zr0}(r,t). \end{aligned} \tag{11}$$

Substituting the displacement and stress expressions of eqns (3)–(8) into the boundary conditions (eqns (9)), and the continuity conditions (eqns (11)), and using eqn (10), the six coefficients A_1, B_1, C_1, D_1, C_0 and D_0 can be determined. Then, the displacements are obtained by substituting A_1, B_1, C_1, D_1, C_0 and D_0 back into eqns (3) and (4)

$$u_i(\rho,\varsigma) = \frac{1}{\mu_1 t}\int_0^\infty \bar{q}(\xi)\left[\bar{u}_i^*(\eta,\varsigma) + \frac{\bar{u}_i(\eta,\varsigma)}{D(\eta)}\right]J_1(\rho\eta)\,\mathrm{d}\eta \tag{12}$$

$$w_i(\rho,\varsigma) = \frac{1}{\mu_1 t}\int_0^\infty \bar{q}(\xi)\left[\bar{w}_i^*(\eta,\varsigma) + \frac{\bar{w}_i(\eta,\varsigma)}{D(\eta)}\right]J_0(\rho\eta)\,\mathrm{d}\eta \tag{13}$$

where

$$\eta = \xi t, \quad \varsigma = z/t, \quad \text{and} \quad \rho = r/t \tag{14}$$

$$D(\eta) = 1-(a+b+4b\eta^2)\,e^{-2\eta} + ab\,e^{-4\eta} \tag{15}$$

$$a = \frac{(3-4\nu_0)\alpha-(3-4\nu_1)}{1+(3-4\nu_0)\alpha}, \quad b = \frac{\alpha-1}{\alpha+(3-4\nu_1)}, \quad \alpha = \frac{\mu_1}{\mu_0} \tag{16}$$

$$\bar{u}_1^*(\eta,\varsigma) = \frac{\varsigma\eta}{8\gamma_0}e^{-\varsigma\eta}, \quad \bar{u}_0^*(\eta,\varsigma) = 0$$

$$\begin{aligned} \bar{u}_1(\eta,\varsigma) = \frac{1}{8\gamma_0}\{&[-4\gamma_0\gamma_2+\gamma_1\varsigma\eta]\,e^{-\varsigma\eta} + [-2\gamma_0(a\varsigma - b\gamma_1\varsigma - 8\gamma_0\gamma_2)\eta \\ &-8b\gamma_0(1-\varsigma)\eta^2 + 4b\varsigma\eta^3]\,e^{-(2+\varsigma)\eta} - ab\varsigma\eta\,e^{-(4+\varsigma)\eta}\} \\ &+\tfrac{1}{4}\{[-(a-b\gamma_1)+2b(2\gamma_2+\varsigma)\eta-4(1-\varsigma)\eta^2]\,e^{-(2-\varsigma)\eta} - 2ab(\gamma_2+\varsigma\eta)\,e^{-(4-\varsigma)\eta}\} \end{aligned}$$

$$\begin{aligned} \bar{u}_0(\eta,\varsigma) = \gamma_0\{&[c-d\gamma_3+2(c-d+d\varsigma)\eta]\,e^{-\varsigma\eta} \\ &+[-ac+bd\gamma_3+2bd(1-\gamma_3-\varsigma)\eta-4bd(1-\varsigma)\eta^2]\,e^{-(2+\varsigma)\eta}\} \end{aligned} \tag{17}$$

$$\bar{w}_1^*(\eta,\varsigma)=\frac{1}{8\gamma_0}(\gamma_1+\varsigma\eta)\,e^{-\varsigma\eta},\quad \bar{w}_0^*(\eta,\varsigma)=0$$

$$\begin{aligned}\bar{w}_1(\eta,\varsigma)=\frac{1}{8\gamma_0}\{&[1+4\gamma_0\gamma_2+\gamma_1\varsigma\eta]\,e^{-\varsigma\eta}+[(a-b\gamma_1)\gamma_2+(a\varsigma-b\gamma_1\varsigma+16b\gamma_0^2)\eta\\&+4b(\gamma_2+2\gamma_0\varsigma)\eta^2+4b\varsigma\eta^3]\,e^{-(2+\varsigma)\eta}-ab(\gamma_1+\varsigma\eta)\,e^{-(4+\varsigma)\eta}\}\\&+\tfrac{1}{4}\{[(a+b\gamma_1)+2b(4\gamma_0-\varsigma)\eta+4b(1-\varsigma)\eta^2]\,e^{-(2-\varsigma)\eta}-2ab(2\gamma_0-\varsigma\eta)\,e^{-(4-\varsigma)\eta}\}\end{aligned}$$

$$\begin{aligned}\bar{w}_0(\eta,\varsigma)=\gamma_0\{&[c+d\gamma_3+2(c-d+d\varsigma)\eta]\,e^{-\varsigma\eta}\\&+[-ac-bd\gamma_3+2bd(1+\gamma_3-\varsigma)\eta-4bd(1-\varsigma)\eta^2]\,e^{-(2+\varsigma)\eta}\}\end{aligned}\tag{18}$$

with

$$\gamma_0=1-\nu_1,\quad \gamma_1=3-4\nu_1,\quad \gamma_2=1-2\nu_1,\quad \gamma_3=3-4\nu_0\tag{19}$$

$$c=\frac{\alpha}{\alpha+\gamma_1},\quad d=\frac{\alpha}{\gamma_3\alpha+1}.\tag{20}$$

When the modular ratio α in eqn (16) is less than 1, the system is said to have a soft film and when $\alpha>1$, it corresponds to a hard coating layer.

The stress components can also be obtained as follows:

$$\begin{aligned}\sigma_{ri}(\rho,\varsigma)=\frac{1}{t^2}\int_0^\infty \bar{q}(\xi)\left[\bar{\sigma}_{ri}^*(\eta,\varsigma)+\frac{\bar{\sigma}_{ri}(\eta,\varsigma)}{D(\eta)}\right]\eta J_0(\rho\eta)\,\mathrm{d}\eta\\-\frac{1}{\rho t^2}\int_0^\infty \bar{q}(\xi)\left[\bar{\sigma}_{ri}^*(\eta,\varsigma)+\frac{\bar{\sigma}'_{ri}(\eta,\varsigma)}{D(\eta)}\right]J_1(\rho\eta)\,\mathrm{d}\eta\end{aligned}\tag{21}$$

$$\sigma_{\theta i}(\rho,\varsigma)=\frac{1}{t^2}\int_0^\infty \bar{q}(\xi)\frac{\bar{\sigma}_{\theta i}(\eta,\varsigma)}{D(\eta)}\eta J_0(\rho\eta)\,\mathrm{d}\eta+\frac{1}{\rho t^2}\int_0^\infty \bar{q}(\xi)\left[\bar{\sigma}_{\theta i}^*(\eta,\varsigma)+\frac{\bar{\sigma}'_{\theta i}(\eta,\varsigma)}{D(\eta)}\right]J_1(\rho\eta)\,\mathrm{d}\eta\tag{22}$$

$$\sigma_{zi}(\rho,\varsigma)=\frac{1}{t^2}\int_0^\infty \bar{q}(\xi)\left[\bar{\sigma}_{zi}^*(\eta,\varsigma)+\frac{\bar{\sigma}_{zi}(\eta,\varsigma)}{D(\eta)}\right]\eta J_0(\rho\eta)\,\mathrm{d}\eta\tag{23}$$

$$\tau_{rzi}(\rho,\varsigma)=\frac{1}{t^2}\int_0^\infty \bar{q}(\xi)\left[\bar{\tau}_{rzi}^*(\eta,\varsigma)+\frac{\bar{\tau}_{rzi}(\eta,\varsigma)}{D(\eta)}\right]\eta J_1(\rho\eta)\,\mathrm{d}\eta\tag{24}$$

where

$$\bar{\sigma}_{r1}^*(\eta,\varsigma)=\tfrac{1}{2}e^{-\varsigma\eta},\quad \bar{\sigma}_{r0}^*(\eta,\varsigma)=0$$

$$\begin{aligned}\bar{\sigma}_{r1}(\eta,\varsigma)=\tfrac{1}{2}\{&[-a+3b+2b(2+\varsigma)\eta-4b(1-\varsigma)\eta^2]\,e^{-(2-\varsigma)\eta}-2ab(1+\varsigma\eta)\,e^{-(4-\varsigma)\eta}\\&-(3-2\varsigma\eta)\,e^{-\varsigma\eta}+2b[2-(2+\varsigma)\eta+2\varsigma\eta^2]\,e^{-(2+\varsigma)\eta}-ab\,e^{-(4+\varsigma)\eta}\}\end{aligned}$$

$$\begin{aligned}\bar{\sigma}_{r0}(\eta,\varsigma)=-\frac{2\gamma_0}{\alpha}\{&[-c+3d-2(c-d(2+\varsigma))\eta]\,e^{-\varsigma\eta}\\&+[ac-3bd+2bd(2+\varsigma)\eta+4bd(1-\varsigma)\eta^2]\,e^{-(2+\varsigma)\eta}\}\end{aligned}$$

$$\begin{aligned}\bar{\sigma}'_{r1}(\eta,\varsigma)=\tfrac{1}{2}\{&[-a+b\gamma_1+2b(2\gamma_2+\varsigma)\eta-4b(1-\varsigma)\eta^2]\,e^{-(2-\varsigma)\eta}-2ab(\gamma_2+\varsigma\eta)\,e^{-(4-\varsigma)\eta}\\&-(\gamma_1-2\varsigma\eta)\,e^{-\varsigma\eta}+2b[2\gamma_0-(2\gamma_2+\varsigma)\eta+2\varsigma\eta^2]\,e^{-(2+\varsigma)\eta}-ab\,e^{-(4+\varsigma)\eta}\}\end{aligned}$$

$$\bar{\sigma}'_{r0}(\eta,\varsigma) = -\frac{2\gamma_0}{\alpha}\{[-c+d\gamma_3-2(c-d(1-\varsigma))\eta]\,e^{-\varsigma\eta} + [ac-bd\gamma_3+2bd(2\gamma_4+\varsigma)\eta+4bd(1-\varsigma)\eta^2]\,e^{-(2+\varsigma)\eta}\} \tag{25}$$

with γ_1, γ_2 and γ_3 given in eqn (19) and $\gamma_4 = 1-2\nu_0$. Also,

$$\begin{aligned}
&\bar{\sigma}^*_{\theta 1}(\eta,\varsigma) = \bar{\sigma}^*_{r1}(\eta,\varsigma), \quad \bar{\sigma}^*_{\theta 0}(\eta,\varsigma) = 0\\
&\bar{\sigma}_{\theta 1}(\eta,\varsigma) = -2\nu_1[-(1+2\eta)b\,e^{-(2-\varsigma)\eta}+ab\,e^{-(4-\varsigma)\eta}+e^{-\varsigma\eta}-(1-2\eta)b\,e^{-(2+\varsigma)\eta}]\\
&\bar{\sigma}_{\theta 0}(\eta,\varsigma) = -\frac{8\nu_0\gamma_0 d}{\alpha}[e^{-\varsigma\eta}-(1-2\eta)b\,e^{-(2+\varsigma)\eta}]\\
&\bar{\sigma}'_{\theta 1}(\eta,\varsigma) = \bar{\sigma}'_{r1}(\eta,\varsigma), \quad \bar{\sigma}'_{\theta 0}(\eta,\varsigma) = \bar{\sigma}'_{r0}(\eta,\varsigma)\\
&\bar{\sigma}^*_{z1}(\eta,\varsigma) = -\bar{\sigma}^*_{r1}(\eta,\varsigma) \quad \bar{\sigma}^*_{z0}(\eta,\varsigma) = 0
\end{aligned} \tag{26}$$

$$\begin{aligned}
\bar{\sigma}_{z1}(\eta,\varsigma) &= \tfrac{1}{2}\{[a+b+2b(2-\varsigma)\eta+4b(1-\varsigma)\eta^2]\,e^{-(2-\varsigma)\eta}-2ab(1-\varsigma\eta)\,e^{-(4-\varsigma)\eta}\\
&\quad -(1+2\varsigma\eta)\,e^{-\varsigma\eta}-2b[(2-\varsigma)\eta+2\varsigma\eta^2]\,e^{-(2+\varsigma)\eta}+ab\,e^{-(4+\varsigma)\eta}\}\\
\bar{\sigma}_{z0}(\eta,\varsigma) &= \frac{2\gamma_0}{\alpha}\{-[c+d+2(c-d(1-\varsigma))\eta]\,e^{-\varsigma\eta}\\
&\quad +[ac+bd-2bd(2-\varsigma)\eta+4bd(1-\varsigma)\eta^2]\,e^{-(2+\varsigma)\eta}\}
\end{aligned} \tag{27}$$

$$\begin{aligned}
&\bar{\tau}^*_{rz1}(\eta,\varsigma) = \bar{\sigma}^*_{z1}(\eta,\varsigma), \quad \bar{\tau}^*_{rz0}(\eta,\varsigma) = 0\\
&\bar{\tau}_{rz1}(\eta,\varsigma) = \tfrac{1}{2}\{[-a+b+2b\varsigma\eta-4b(1-\varsigma)\eta^2]\,e^{-(2-\varsigma)\eta}-2ab\varsigma\eta\,e^{-(4-\varsigma)\eta}\\
&\qquad +(1-2\varsigma\eta)\,e^{-\varsigma\eta}-2b(1-\varsigma\eta+2\varsigma\eta^2)\,e^{-(2+\varsigma)\eta}+ab\,e^{-(4+\varsigma)\eta}\}\\
&\bar{\tau}_{rz0}(\eta,\varsigma) = \frac{2\gamma_0}{\alpha}\{-[c-d+2(c-d(1-\varsigma))\eta]\,e^{-\varsigma\eta}\\
&\qquad +[ac-bd+2bd\varsigma\eta+4bd(1-\varsigma)\eta^2]\,e^{-(2+\varsigma)\eta}\}.
\end{aligned} \tag{28}$$

For a given loading condition on the film surface (Fig. 1), the elastic field can be solved by the inversion of Hankel's transform. Due to the complexity of the integral involved in the inversion, it is not feasible to derive an analytical solution. However, numerical integration can be readily carried out with IMSL subroutines to determine the displacement and stress fields. It should be noted that when the boundary condition $q(r)$ is reduced to a *point* force, the present solution coincides with that of Chan *et al.* (1974), and it further becomes the exact solution of a point force for a homogeneous half space with $\alpha = 1$ and $\nu_1 = \nu_0$.

3. NUMERICAL RESULTS

To simulate the nonlinear loading distribution that often arises in the indentation problems, the distribution of surface loading is assumed to take the following form:

$$q(r) = \begin{cases} \sigma_m\left[1-\left(\dfrac{r}{r_0}\right)^2\right]^n & r \leqslant r_0\\ 0 & r > r_0 \end{cases} \tag{29}$$

where σ_m is the maximum stress at $r = 0$, and r_0 is the loading contact radius. When the parameter $n = 0$, the distribution of the surface loading becomes a uniform pressure. The

Hertzian contact stress can be obtained when $n = 1/2$. Since the distribution of the surface loading is not known precisely for the coating/substrate systems and most indentation tests do not have uniform pressure on the surface, we assume $n = 1$ in the following numerical calculations for the reason of simplicity. As will be shown later, the functional form of eqn (29) is capable of simulating a wide variety of indentation profiles. Then this boundary condition can be written in Hankel's transform as

$$\bar{q}(\xi) = 2\frac{\sigma_m t^2}{\rho_0}\left[\frac{2}{\eta^3}J_1(\rho_0\eta) - \frac{\rho_0}{\eta^2}J_0(\rho_0\eta)\right] \tag{30}$$

where $\rho_0 = r_0/t$. Substituting eqn (30) into eqns (12), (13) and (21)–(24), the displacement and stress fields can be obtained in terms of the thickness of the film and the elastic properties of the film and the substrate. The results of the analysis for different coating materials are summarized below in terms of the profile of the displacement on the free surface, the stress field of the system, and the variation of the total applied load P with the depth of the indentation.

In the following discussions we adopt the terms *hard-coating* and *soft-coating* to identify the coating/substrate systems for which $\alpha = \mu_1/\mu_0 > 1$ and < 1, respectively. $\alpha = 1$ represents a homogeneous material.

3.1. *Displacement profile of the film surface*

The displacement profile of the film *surface* under the axisymmetric compressive loading is of considerable interest. At the surface, $z = 0$, the displacement can be expressed as

$$\frac{\mu_1}{2\sigma_m}\frac{w(\rho,0)}{r_0} = \int_0^\infty \frac{1}{\rho_0^2}\left[\frac{2}{\eta^3}J_1(\rho_0\eta) - \frac{\rho_0}{\eta^2}J_0(\rho_0\eta)\right]\frac{1+4b\eta e^{-2\eta} - ab e^{-4\eta}}{D(\eta)}J_0(\rho\eta)\,\mathrm{d}\eta. \tag{31}$$

When $\alpha = 1$, $a = b = 0$, and $D = 1$, the integration in eqn (31) can be obtained in closed form, and the result reduces to the analytical solution of a homogeneous half-space under axisymmetric loading P.

To uncover the effect of material properties on the response of the coating/substrate system, we have varied the ratio of shear moduli, $\alpha = \mu_1/\mu_0$, and assumed $\nu_1 = \nu_0 = 0.33$ in the numerical calculations. Figures 2(a)–(c) show the displacement profiles of the film surface vs α and t. Here the substrate is chosen as a reference phase, and the elastic property of the film is changed with respect to that of the substrate. We normalize the surface displacement $w(\rho,0)$ as $\mu_0 w/(2\sigma_m r_0)$ and the radius r as r/r_0. The non-dimensional displacement curves vs the non-dimensional radius on the film surface ($z = 0$) are shown in Fig. 2(a) for the ratio of shear moduli $\alpha = 10$, 1 and 0.1, with a film thickness equal to half of the loading contact radius ($t/r_0 = 0.5$). As the shear modular ratio α decreases from 10 to 0.1, the film surface deformation increases significantly in the loading contact region $r < r_0$. The displacement profiles readily converge outside of the contact region and vanish as $r \to \infty$.

Figures 2(b) and (c) show the influence of the film thickness on the displacement profiles of the film surface with a hard and a soft coating, respectively. In Fig. 2(b) the solid lines represent the film surface displacements for three different film thicknesses: $t/r_0 = 0.1$, 1 and 10. Also shown, as the chain-dotted lines, are the displacement profiles of the individual film material ($t/r_0 \to \infty$) and substrate ($t/r_0 \to 0$). These two cases provide the upper and lower bounds of the vertical displacement of the film/substrate system. When the film thickness is large compared to the contact radius, the result approaches that of the individual film material. In contrast, the surface displacement profile approaches that of the substrate material alone, as the film thickness is very small compared to the loading contact radius. With a soft coating, the influence of the film thickness on the surface displacement of the two-phase system (Fig. 2(c)) is reversed. The surface displacement of

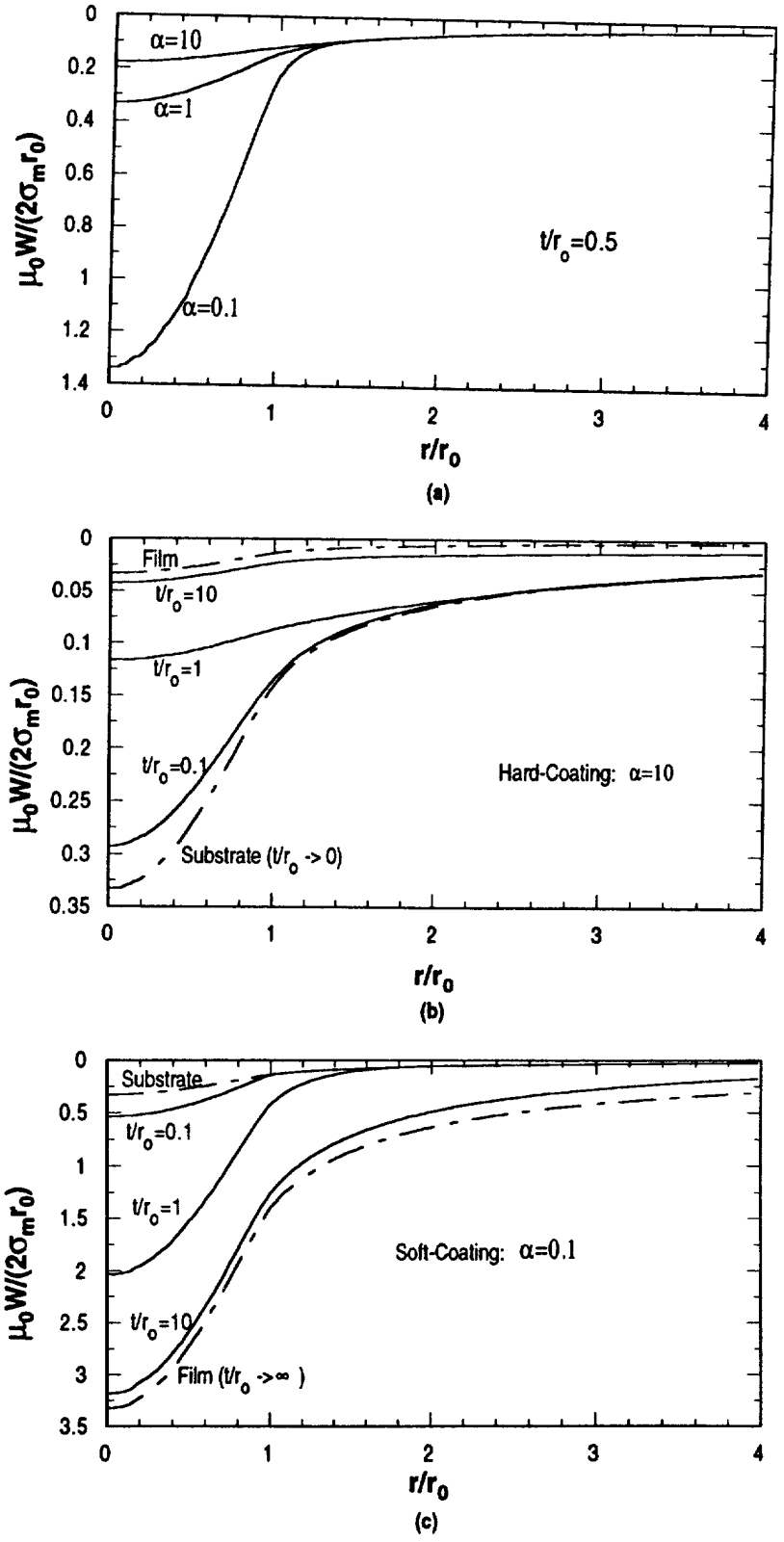

Fig. 2. Surface displacement profiles of a coating/substrate system as affected by load: (a) the shear modulus ratio, (b) the hard-coating film thickness, and (c) the soft-coating film thickness.

the coating/substrate system with various film thicknesses again is bounded by the two limit cases.

3.2. *Stress distribution*

Knowledge of the stress field (eqns (21)–(24)) is relevant to the understanding of the failure mechanisms of the coating/substrate system. Figures 3(a) and (b) show the variations of the stress components as a function of depth along the z-axis for $t/r_0 = 1$. The radial and hoop stresses are equal due to symmetry (Fig. 3(a)). The maximum compressive stresses occur at the film surface for all three systems. The discontinuity of radial (and hoop) stress exists across the interface (indicated by the horizontal dash-dot line at $z/t = 1$ in Fig. 3(a)) for both soft- and hard-coating systems because of the mismatch of the elastic modulus. Furthermore, the radial (and hoop) stress component is compressive for both the soft-coating/substrate system and the substrate alone. For the hard-coating/substrate system, the radial (and hoop) stress changes from maximum compression at the surface to maximum

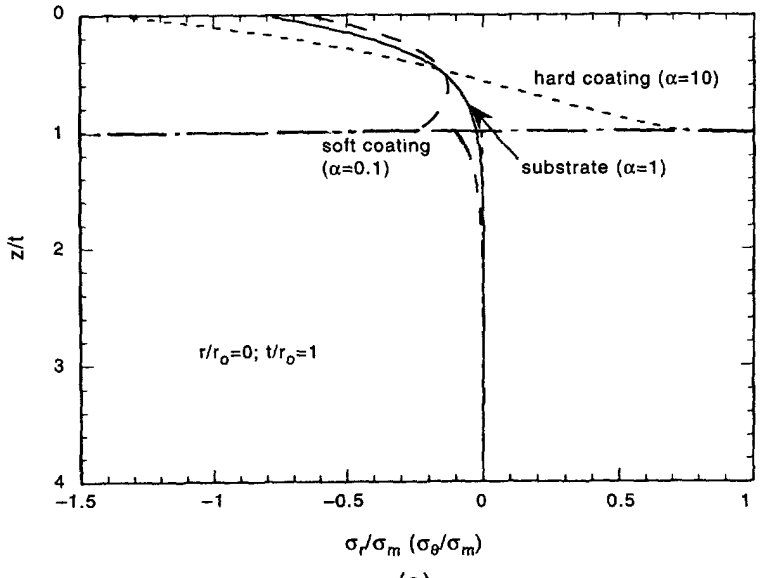

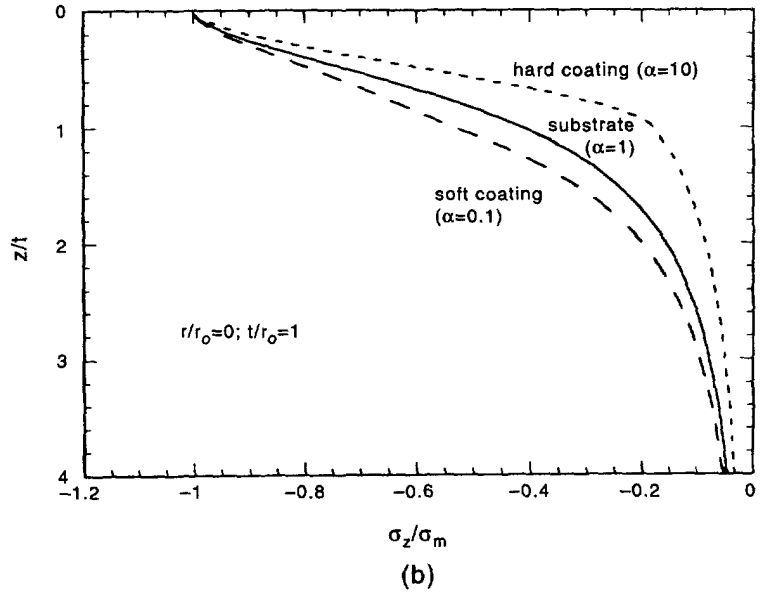

Fig. 3. Stress distributions along the z-axis.

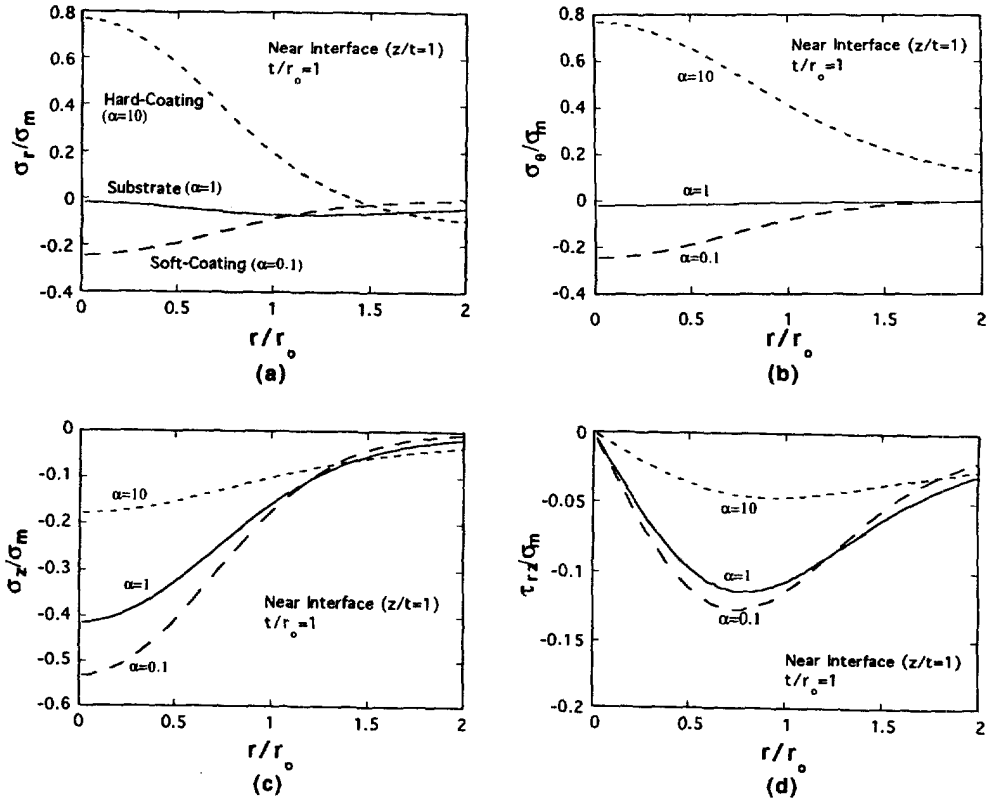

Fig. 4. Stress distributions at the interface with the thickness of the film $t = r_0$.

tension right above the interface, then jumps to a very small value and approaches zero as $z \to \infty$. Figure 3(b) shows the variation of normal stress σ_z with z. σ_z is compressive and maximum (σ_m) at the film surface, then decays to zero as $z \to \infty$ for both hard and soft coatings. The soft-coating system experiences higher σ_z than the hard-coating system. Due to the traction continuity conditions at the interface, there is no discontinuous for σ_z in Fig. 3(b). The shear stress σ_{rz} vanishes along the line $r = 0$ since the symmetry.

It is evident from Fig. 3(a) that there exist discontinuities of the stress near the film/substrate interface, which may lead to delamination and interfacial fracture. It is therefore desirable to have a full stress profile of the interfacial region. Figures 4(a)–(d) show the variations of σ_r, σ_θ, σ_z and τ_{rz} as a function of radial distance r in the thin film for $t = r_0$ and $z = t$. Figures 4(a) and (b) indicate that both the radial and the hoop stresses within the contact zone ($r \leqslant r_0$) are tensile for the hard-coating case and compressive for the soft-coating case. These components gradually decrease to zero as $r \to \infty$. Figure 4(c) shows that the compressive stress σ_z is more pronounced in a soft-coating system below the indentation zone, but outside of this zone the stress field is not sensitive to the elastic property of the film. The shear stress distribution is given in Fig 4(d), which vanishes at the origin. The maximum shear stress occurs near the edge of the loading zone, around $r/r_0 = 0.75$ for the soft-coating, and around 0.9 for the hard-coating.

Next, we examine the influence of the film thickness on the stress field. Figures 5(a) and (b) show the dependence of stress components on the film thickness t at two critical interface locations, $r/r_0 = 0$ and 1, for a hard-coating system ($\alpha = 10$). At $r = 0$, Fig. 5(a) shows that the radial and hoop stresses are identical in magnitude and compressive when the film thickness is very thin ($t/r_0 < 0.1$). Both stresses become tensile as the film thickness increases, reach the maximum at $t/r_0 \approx 0.35$, and decay to the values which exist in the half-space of the film material as $t \to \infty$. The normal stress σ_z is compression and higher for a thinner film. The shear stress τ_{rz} remains zero at $r = 0$ because of the symmetry condition.

At the interface location $r = r_0$, Fig. 5(b) shows that σ_r and σ_θ are not longer identical in magnitude within the film thickness range of approximately $t < 4r_0$. The shear stress τ_{rz}

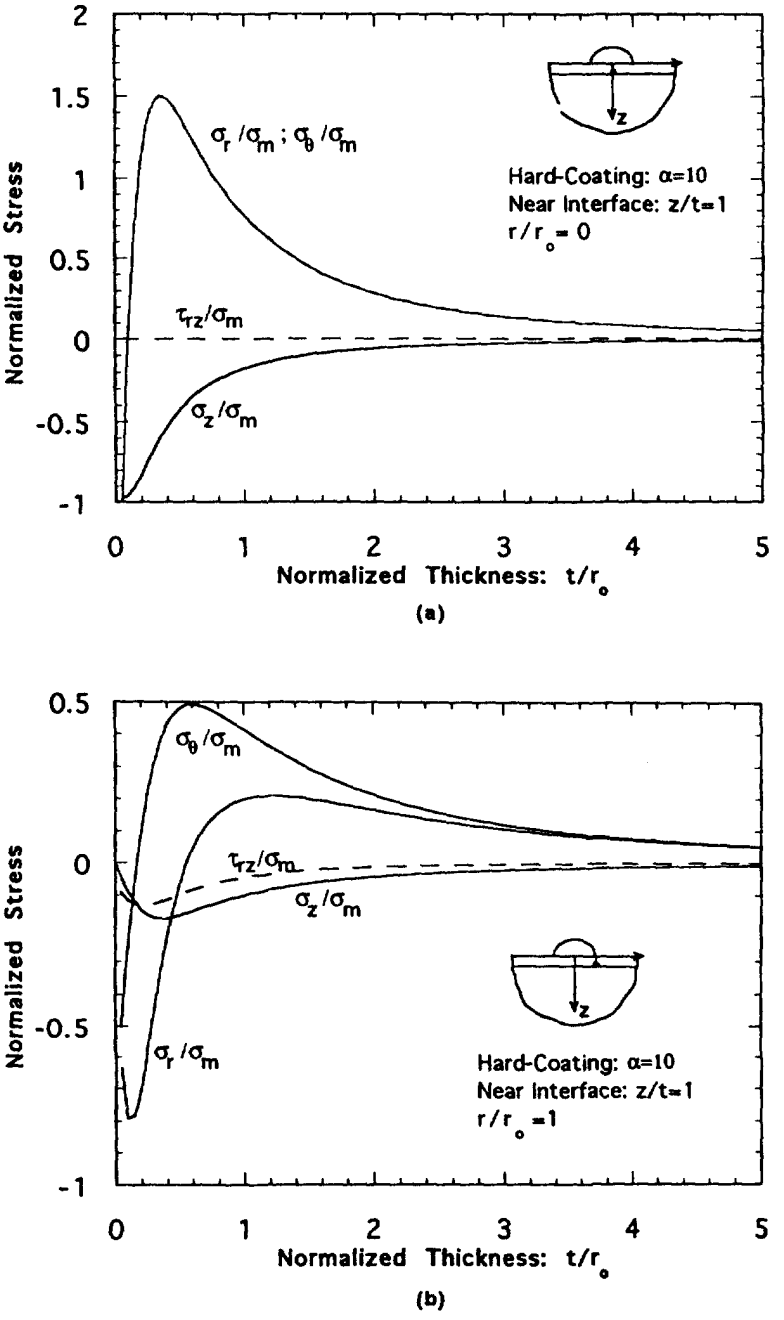

Fig. 5. The relations between the stress components and the film thickness for a hard-coating/substrate system, $\alpha = 10$.

is appreciable for $t \leqslant r_0$. The compressive normal stress σ_z increases in magnitude with the film thickness initially and then diminishes as the thickness further increases.

For comparison with Figs 5(a) and (b), the influence of the film thickness on the stress components at the interface locations $r = 0$ and $r = r_0$ for a soft-coating system ($\alpha = 0.1$) is shown in Figs 6(a) and (b). The significant difference between the hard-coating and soft-coating systems is that both the radial and hoop stresses in a soft-coating system are compressive regardless of the film thickness, while they may be tensile in a hard-coating system. Figure 6(a) shows that all the normal stresses assume maximum values at $t = 0$ for $r = 0$. However, the peak normal stresses occur at $t/r_0 = 1$ for $r = r_0$ (Fig. 6(b)). Also, significant τ_{rz} develops near the interface at $t/r_0 = 1$ for $r = r_0$.

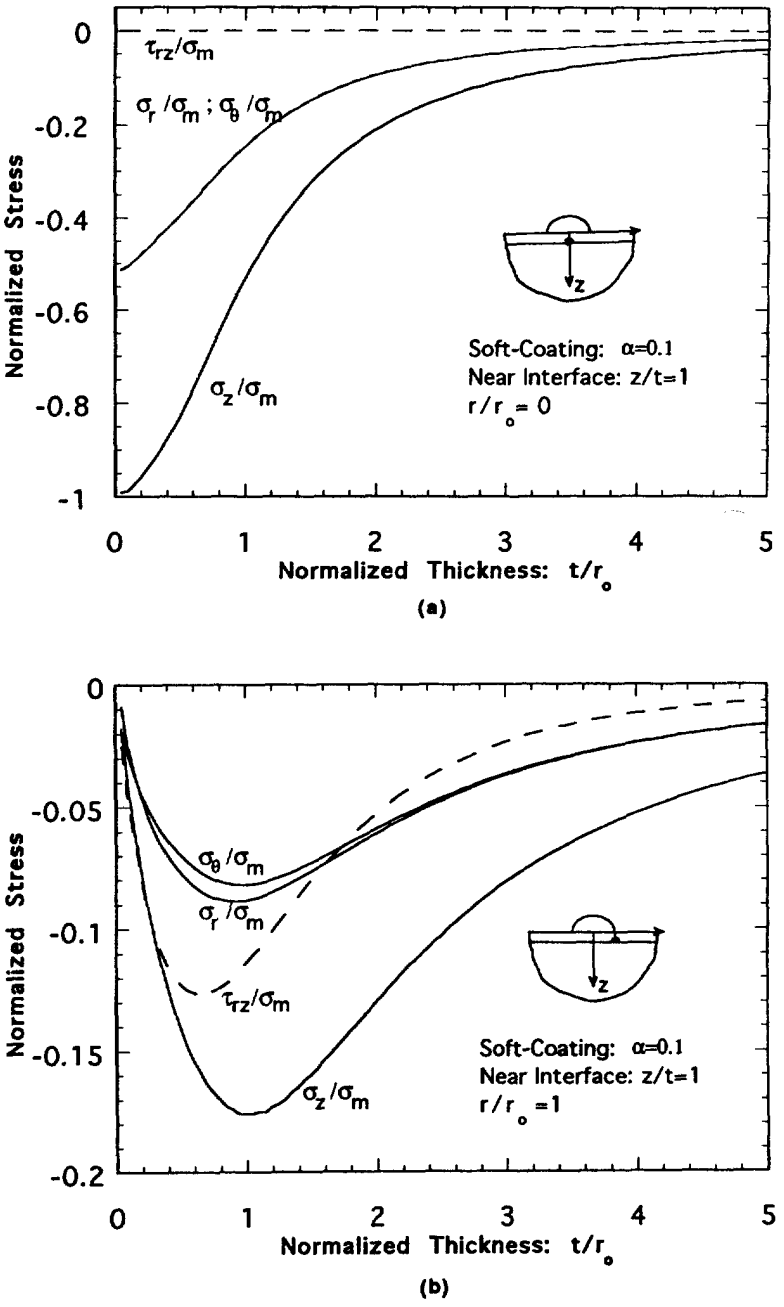

Fig. 6. The relations between the stress components and the film thickness for a soft-coating/substrate system, $\alpha = 0.1$.

In order to put the present analysis of the coating/substrate system in perspective, it is useful to compare the analytical stress fields with existing results obtained by finite element method. Figures 7(a) and (b) show the comparison of the interfacial normal and shear stresses of the coating/substrate system with the finite element calculations by Jayachandran *et al.* (1995). In their paper, the coating material is polymethymethacrylate (PMMA) with the elastic properties of $E_1 = 3.25$ GPa and $\nu_1 = 0.30$, and the substrate is taken to be rigid ($\alpha = 0$). The dots and the filled triangles are finite element solutions and the solid lines indicate the theoretical solutions for the indentation depth normalized by the film thickness ($d/t = 0.06$ and 0.24). The normal stress results (here the positive value indicates the magnitude of the compressive normal stress) in Fig. 7(a) are in good agreement when $r/r_0 \leqslant 0.7$. It should be noted that in the finite element analysis by Jayachandran *et al.*

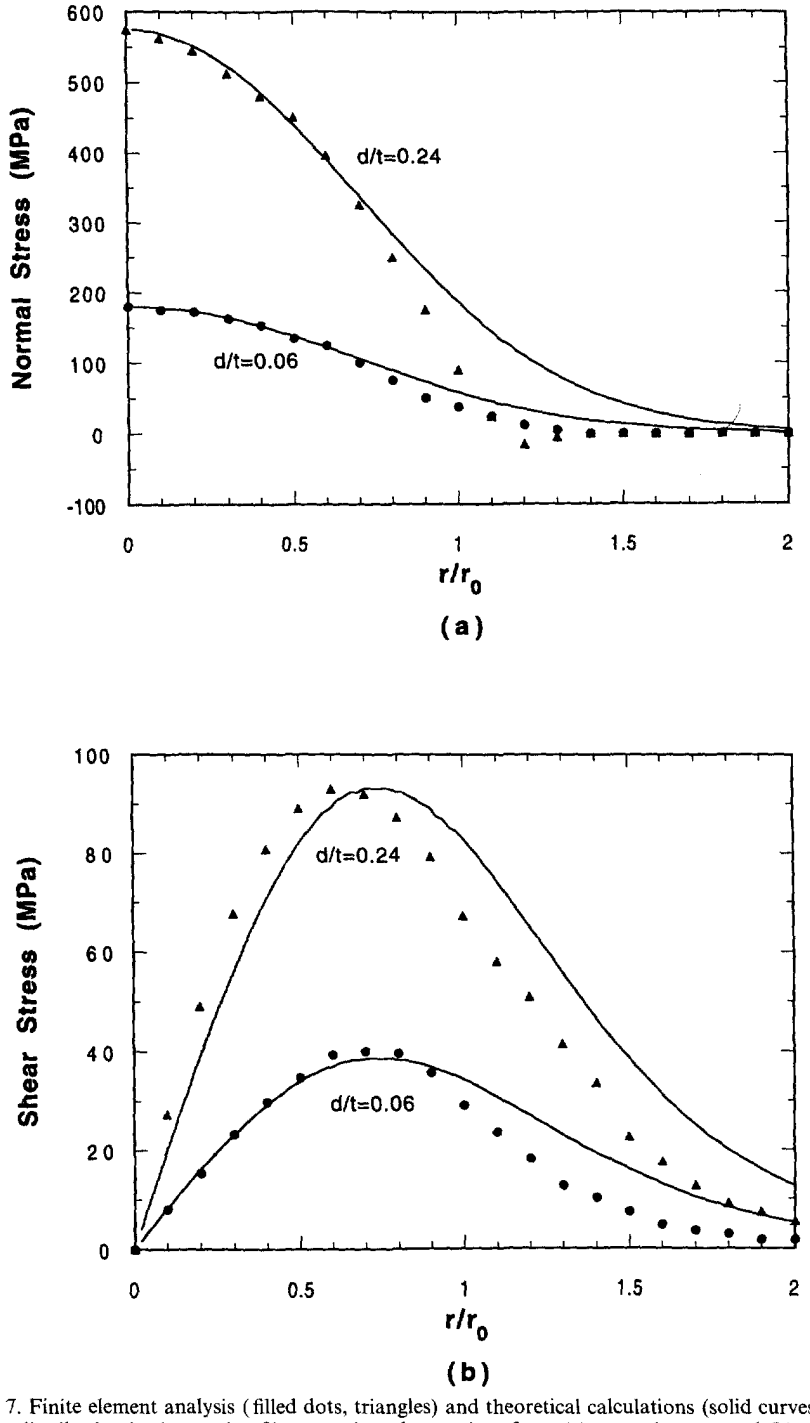

Fig. 7. Finite element analysis (filled dots, triangles) and theoretical calculations (solid curves) of stress distribution in the coating film near the substrate interface: (a) normal stress, and (b) shear stress.

(1995), the pile-up around the loading contact radius and the elastic–viscoplastic effects have been accounted for. However, the present theoretical analysis is only for the elastic case without considering the pile-up at the edge of the contact zone. These differences will obviously affect the stress solutions, especially when r approaches the edge of the contact zone (r_0), and the indentation depth is high. The shear stress fields in Fig. 7(b) from these two approaches also show some difference when $r/r_0 > 1$ for $d/t = 0.06$; for $d/t = 0.24$, the theoretical calculation and finite element analysis show the same trend but somewhat different values.

3.3. *Relation between total load* P *and depth of indentation* d

It was assumed in eqn (29) that the normal stress distribution on the film surface follows a parabolic function of the radial distance. Based upon such a stress boundary condition, the displacement and the stress fields have been obtained. In this section, we consider the relation between the total applied load P and the depth of indentation d of the coating/substrate system. The analysis in the following again is limited to the idealized static problem; the dynamic effect, large deformation and plastic flow, often encountered in indentation problems, are neglected.

First, the total indentation force is derived from the contact area and normal stress (eqn (29)):

$$P = 2\pi \int_0^{r_0} rq(r)\,\mathrm{d}r = \frac{\pi}{2}\sigma_m r_0^2. \tag{32}$$

The maximum stress σ_m and the loading contact radius r_0 change from zero to certain values as the indentation load changes. Harding and Sneddon (1945) found that the total load P is proportional to r_0^3 for a homogeneous half-space under a rigid spherical indentation. As an assumption, we also choose the total load P to be proportional to r_0^3. This results in a linear relation between the maximum stress σ_m and the loading contact radius r_0 as follows:

$$\sigma_m = \sigma_0 \frac{r_0}{t}, \tag{33}$$

where σ_0 is a constant reference stress and t the thickness of the film as a reference length. Substituting eqn (33) into eqn (32), the total load can be rewritten as

$$P = \frac{t^2 \pi \sigma_0}{2} \rho_0^3, \tag{34}$$

where $\rho_0 = r_0/t$. The penetration depth, $d = w(0,0)$, of the indenter is then obtained from eqn (31)

$$\frac{\mu_0}{2\sigma_0}\frac{d}{t} = \int_0^\infty \left[\frac{2}{\eta^3} J_1(\rho_0\eta) - \frac{\rho_0}{\eta^2} J_0(\rho_0\eta)\right] \frac{1 + 4b\eta\, e^{-2\eta} - ab\, e^{-4\eta}}{\alpha D(\eta)}\,\mathrm{d}\eta. \tag{35}$$

Figure 8 shows the non-dimensional total load vs the depth of the indentation in terms

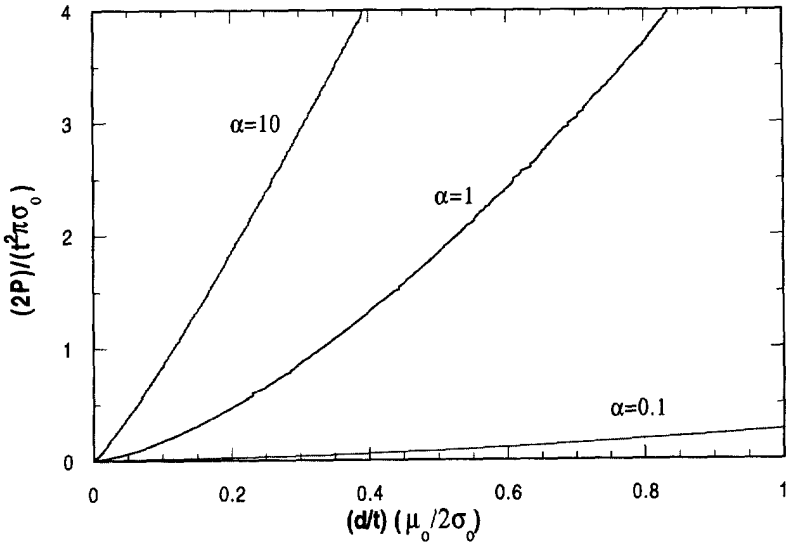

Fig. 8. Variation of the total load, P with the depth of indentation d.

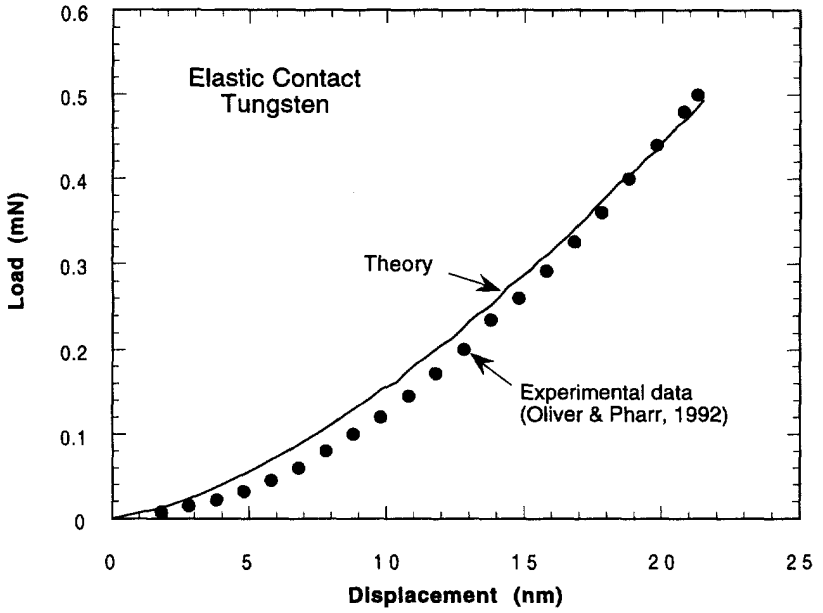

Fig. 9. Experimental (solid circles) and theoretical (solid line) results of the load-indentation depth relation for elastic indentation of tungsten.

of the ratio of the shear modulus of the film to that of the substrate, α. All results exhibit the nonlinear relations between P and d. This nonlinear behavior has been observed in indentation experiments (see, for example, Matthewson, 1981; Doerner and Nix, 1986; Ritter *et al.*. 1989; Lin *et al.*, 1990; and Oliver and Pharr, 1992).

Finally the load-indentation depth relation is compared with experimental data for tungsten subjected to elastic indentation obtained by Oliver and Pharr (1992). The elastic properties of tungsten are given as $E = 410$ GPa and $\nu = 0.280$. The experimental data of tungsten are shown as filled circles in Fig. 9, and the theoretical result is indicated by the solid line. The good comparison indicates that the assumptions made in the present analysis are adequate in representing the load-indentation depth relations on the film/substrate systems.

4. DISCUSSIONS AND CONCLUSIONS

An elastic analysis has been performed to determine the displacement and stress fields of thin-film coating/substrate systems subjected to an axisymmetric contact loading. It is assumed that the elastic surface layer and substrate are perfectly bonded. The contact loading area and film thickness are allowed to vary. By changing the ratio of the shear moduli of the surface film and substrate, the layered half-space is intended to simulate the hard-coating/soft-substrate and soft-coating/hard-substrate systems. The elastic field due to a parabolic compressive loading has been obtained. The displacement profiles on the film surface and the stress distributions within the coating have been found to be highly sensitive to both the film thickness and the elastic properties of the film and the substrate. In general, the substrate can not be treated as rigid.

The displacement profiles imply that when the film thickness is sufficiently large compared to the contact radius, the elastic solution approaches that of a half-space problem. Sneddon's solution for the half-space punch problem can then be used to measure the elastic property of the film by a nano-indentation technique. On the other hand, if the film thickness is insufficient, the elastic property of the film determined by Sneddon's indentation solution is inaccurate due to the influence of the substrate. In this case, a new solution method needs to be found to determine the film elastic property.

The analytical results also indicate significant differences in the stress distributions between the hard-coating and soft-coating/substrate systems, which may give rise to different failure mechanisms. At the interface and within the loading contact zone, the radial and hoop stresses are tensile for the hard-coating system and compressive for the soft-coating system. The shear stress reaches the maximum value near the edge of the contact zone ($r \approx r_0$) for both hard-coating and soft-coating systems. It can be concluded from this study that cracking of the surface film and interfacial debonding can occur in the hard-coating/substrate system, while interfacial debonding is the key failure mechanism in the soft-coating/substrate system. The present findings are consistent with the analytical prediction of Matthewson (1981) regarding interfacial debonding for the soft-coating systems and the corresponding experimental observations of Ritter *et al.* (1989) and Lin *et al.* (1990).

Acknowledgements—This work was supported by the U.S. Army Research Laboratory. We are grateful to Dr M. R. Fletcher for the guidance and encouragement in the course of this research.

REFERENCES

Chan, K. S., Karasudhi, K. and Lee, S. L. (1974) Force at a point in the interior of a layered elastic half space. *International Journal of Solids and Structures* **10,** 1179–1199.

Chui, Y. P. and Hartnett, M. J. (1983) A numerical solution for layered solid contact problems with application to bearings. *ASME Journal of Lubrication Technology* **105,** 585–590.

Doerner, M. F. and Nix, W. D. (1986) A method for interpreting the data from depth-sensing indentation instruments. *Journal of Material Research* **1**(4), 601–609.

Harding, J. W. and Sneddon, I. N. (1945) The elastic stresses produced by the indentation of the plane surface of a semi-infinite elastic solid by a rigid punch. *Proceedings of the Cambridge Philosophical Society* **41,** 16–26.

Jayachandran, R., Boyce, M. C. and Argon, A. S. (1995) Mechanics of the indentation test and its use to assess the adhesion of polymeric coatings. In *Adhesion Measurement of Films and Coatings*, ed. K. L. Mittal. VSP, pp. 189–215.

Johnson, K. L. (1985) *Contact Mechanics*. Cambridge University Press.

Komvopoulos, K., Saka, N. and Suh, N. P. (1987) The role of hard layers in lubricated and dry sliding. *ASME Journal of Tribology* **109,** 223–231.

Komvopoulos, K. (1988) Finite element analysis of a layered elastic solid in normal contact with a rigid surface. *ASME Journal of Tribology* **110,** 477–485.

Komvopoulos, K. (1988) Elastic–plastic finite element analysis of indented layered media. *ASME Journal of Tribology* **111,** 430–439.

Kral, E. R., Komvopoulos, K. and Bogy, D. B. (1995) Finite element analysis of repeated indentation of an elastic–plastic layered medium by a rigid sphere, Part I. Surface results. *ASME Journal of Applied Mechanics* **62,** 20–28.

Kral, E. R., Komvopoulos, K. and Bogy, D. B. (1995) Finite element analysis of repeated indentation of an elastic–plastic layered medium by a rigid sphere, Part II. Subsurface results. *ASME Journal of Applied Mechanics* **62,** 29–42.

Lardner, T. J., Giovinazzo, R. J. and Ritter, J. E. (1992) The effect of high modulus single and double layer coatings on contact stress. *Philosophical Magazine A* **66,** 437–455.

Lin, M. R., Ritter, J. E., Rosenfeld, L. and Lardner, T. J. (199) Measuring the interfacial shear strength of thin polymer coatings on glass. *Journal of Material Research* **5**(5), 1110–1117.

Matthewson, M. J. (1981) Axis-symmetric contact on thin compliant coatings. *Journal of the Mechanics and Physics of Solids* **29**(2), 89–113.

Oliver, W. C. and Pharr, G. M. (1992) An improved technique for determining hardness and elastic modulus using load and displacement sensing indentation experiments. *Journal of Material Research* **7**(6), 1564–1583.

O'Sullivan, T. C. and King, R. B. (1988) Sliding contact stress field due to a spherical indenter on a layered elastic half-space. *ASME Journal of Tribology* **110,** 234–240.

Ritter, J. E., Lardner, T. J., Rosenfeld, L. and Lin, M. R. (1989) Measurement of adhesion of thin polymer coatings by indentation. *Journal of Applied Physics* **66**(8), 3626–3634.

Sneddon, I. N. (1948) Boussinesq's problem for a rigid cone. *Proceedings of the Cambridge Philosophical Society* **44,** 492–507.

Sneddon, I. N. (1951) *Fourier Transforms*. McGraw-Hill, New York.

Sneddon, I. N. (1965) The relation between load and penetration in the axisymmetric Boussinesq problem for a punch of arbitrary profile. *International Journal of Engineering Science* **3,** 47–57.

Van der Zwaag, S. and Field, J. E. (1982) The effect of thin hard coatings on the Hertzian stress field. *Philosophical Magazine A* **46,** 133–150.

Van der Zwaag, S. and Field, J. E. (1983) Indentation and liquid impact studies on coated germanium. *Philosophical Magazine A* **48,** 767–777.

Van der Zwaag, S., Dear, J. P. and Field, J. E. (1986) The effect of double layer coatings of high modulus on contact stresses. *Philosophical Magazine A* **53,** 101–111.